JACS Au
AN OPEN ACCESS JOURNAL OF THE AMERICAN CHEMICAL SOCIETY

pubs.acs.org/jacsau

Article

A Highly Selective Mn(II)-Specific DNAzyme and Its Application in Intracellular Sensing

Huanhuan Fan,* Claire E. McGhee, Ryan J. Lake, Zhenglin Yang, Zijian Guo, Xiao-Bing Zhang,* and Yi Lu*

Cite This: *JACS Au* 2023, 3, 1615−1622

Read Online

ACCESS | Metrics & More | Article Recommendations | Supporting Information

ABSTRACT: Manganese is an essential trace element in the human body that acts as a cofactor in many enzymes and metabolisms. It is important to develop methods to detect Mn^{2+} in living cells. While fluorescent sensors have been very effective in detecting other metal ions, Mn^{2+}-specific fluorescent sensors are rarely reported due to nonspecific fluorescence quenching by the paramagnetism of Mn^{2+} and poor selectivity against other metal ions such as Ca^{2+} and Mg^{2+}. To address these issues, we herein report in vitro selection of an RNA-cleaving DNAzyme with exceptionally high selectivity for Mn^{2+}. Through converting it into a fluorescent sensor using a catalytic beacon approach, Mn^{2+} sensing in immune cells and tumor cells has been achieved. The sensor is also used to monitor degradation of manganese-based nanomaterials such as MnOx in tumor cells. Therefore, this work provides an excellent tool to detect Mn^{2+} in biological systems and monitor the Mn^{2+}-involved immune response and antitumor therapy.

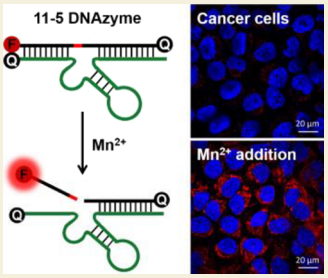

KEYWORDS: *in vitro selection, DNAzymes, Mn^{2+}, high selectivity, fluorescence imaging*

INTRODUCTION

Manganese is an essential metal ion in all forms of life by playing key roles in a wide range of biological processes.[1] For example, manganese participates as a cofactor in diverse classes of enzymes, especially manganese catalase (MnCAT) and manganese superoxide dismutase (MnSOD).[2−4] In recent years, Mn^{2+} has been shown to be directly activate cGAS or increase the sensitivity of cGAS to double-stranded DNA and augment STING activation in innate immunity, which is critical for the host defense against DNA viruses.[5,6] Moreover, an increasing number of manganese-based nanomaterials are developed and widely used in antitumor therapy based on their good response to the tumor microenvironment, which is always accompanied by the production of large amounts of Mn^{2+}.[7−10] However, disorder of manganese metabolism, especially excessive intake of manganese, could cause severe neurological damages, such as Parkinson's disease.[11] Given the presence of Mn^{2+} in many biological processes and the risk of manganese intoxication, it is necessary to develop Mn^{2+} sensors to probe the location and distribution of Mn^{2+} in biological systems.

To image metal ions in biological systems, fluorescent sensors have been widely used due to their advantages of high sensitivity, subcellular resolution, and rapid response.[12,13] As a result, a number of fluorescent probes have been developed for detecting diverse metal ions in living cells, such as Ca^{2+},[14,15] Mg^{2+},[16−18] Zn^{2+},[19−21] Cu^{2+},[22−24] and Fe^{2+}.[25] Mn^{2+}-specific fluorescent sensors, however, are rarely reported. One major issue is that paramagnetic nature of Mn^{2+} could induce nonspecific fluorescence quenching,[26,27] which makes it difficult to design Mn^{2+}-responsive fluorescent molecular probes. To address this issue, genetically encoded fluorescent sensors for Mn^{2+} engineered from lanmodulin, called MnLaMP1 and MnLaMP2, have recently been reported.[28] While it is an exciting advance in the field, the reported selectivities of MnLaMP1 against Ca^{2+}, Mg^{2+}, and Zn^{2+} are 5.5-, 48-, and 0.3- fold, respectively. Considering that cellular labile Mn^{2+} concentration is normally in a low micromolar range, while Ca^{2+} in the endoplasmic reticulum (ER) can reach hundreds of micromolar level[29] and Mg^{2+} in many cell locations can reach the millimolar level,[30] the application of MnLaMP1 is limited to imaging Mn^{2+} in bacteria, and it has not been successfully applied to mammalian cells. Further endeavor in improving the selectivity resulted in MnLaMP2,[28] but the drifted FRET response and higher background in detection have prevented this selective sensor from being applied for any cellular imaging. Therefore, it is very important to develop Mn^{2+}-specific fluorescent "turn-on" sensors with high selectivity and a tunable response range for cellular and in vivo applications.

To overcome the above limitations, we are interested in developing DNAzyme-based fluorescent sensors. DNAzymes, a class of DNA molecules that display enzymatic activity such as

Received: February 8, 2023
Revised: April 20, 2023
Accepted: May 1, 2023
Published: May 15, 2023

https://doi.org/10.1021/jacsau.3c00062
JACS Au 2023, 3, 1615−1622

RNA cleavage,[31−33] were first discovered by Breaker and Joyce in 1994 through a combinatorial process called in vitro selection.[34] Using this strategy, we and others have selected many metal ion-specific DNAzymes and turned them into fluorescent sensors, including UO_2^{2+},[35,36] Zn^{2+},[37,38] Pb^{2+},[39] Mg^{2+},[40,41] Co^{2+},[42] Cu^{2+},[43] Cd^{2+},[44] Hg^{2+},[45] Ag^{+},[46] Na^{+},[47,48] Li^{+},[49] Cr^{3+},[50] and lanthanides.[51] A major advantage of DNAzymes for sensing metal ions is that they can be acquired without prior knowledge of specific metal−DNA interaction or potential metal ion binding sites because metal-specific DNAzymes can be selected from a large library of DNA molecules,[52] similar to small-molecule DNA aptamer isolation.[53,54] In addition, the binding affinity of specific metal ions to the potential DNAzymes can be enhanced by tuning the stringency of selection pressure for a tunable dynamic range,[55] while the metal selectivity can be improved by introducing negative or counter selection against competing metal ions through the in vitro selection process.[56,57] More importantly, these DNAzymes can be converted into fluorescent sensors using a catalytic beacon approach that allows separation of the metal-binding site and fluorophore,[58,59] avoiding the metal-based fluorescence quenching and resulting in fluorescence turn-on sensors. Finally, their good biocompatibility makes DNAzyme-based fluorescent sensors an ideal tool for detecting metal ions in living cells.

In this study, we report in vitro selection and characterization of an RNA-cleaving DNAzyme with exceptionally high selectivity for Mn^{2+} over other competing metal ions, especially Ca^{2+} and Mg^{2+}. We converted it into a fluorescent turn-on sensor based on the catalytic beacon approach and demonstrated its good activity and selectivity in the selection buffer. Through adopting an efficient DNAzyme delivery method by lipofectamine 3000, Mn^{2+} sensing in immune cells and tumor cells was achieved. Degradation of manganese-based nanomaterials such as MnOx in tumor cells was also observed. Therefore, this work provides an excellent tool for Mn^{2+} detection in biological systems and monitoring of the Mn^{2+}-involved immune response and antitumor therapy.

RESULTS AND DISCUSSION

In Vitro Selection of Mn^{2+}-Specific DNAzymes

To acquire Mn^{2+}-specific DNAzymes, we carried out a gel-based in vitro selection using a method reported previously.[35,47] A 110-mer oligonucleotide containing a 50-nt random sequence was designed as the selection library (Figure S1). A single adenosine ribonucleotide (rA) was incorporated in the 5′-conserved region as the intended cleavage site. Two distinct pairing regions were designed to confine the folded random region to be in proximity of the rA cleavage site. The selection procedure was performed as shown in Figure S2. Initially, the selection pools were incubated in selection buffer (50 mM Bis-Tris, 300 mM NaCl, pH 6.8) for 2 h as the negative selection to remove DNAzymes that would cleave or degrade in the buffer. Uncleaved DNA sequences were purified by the polyacrylamide gel electrophoresis (PAGE) and further incubated with 500 μM Mn^{2+} for 2 h as the positive selection. Next, two steps of PCR amplification were carried out to regenerate selection pools for the next round of selection. To improve the selectivity of the selection pools to Mn^{2+} over other competing divalent metal ions, from Round 8, the negative selection was replaced with counter selection, which selects against the metal mix of those competing metals (500 μM Zn^{2+}, 500 μM Cu^{2+}, 100 μM Pb^{2+}, 10 mM Mg^{2+}, and 10 mM Ca^{2+}). To search for more efficient DNAzymes, we gradually decreased the positive reaction time from 2 to 0.5 h to improve the selection stringency (Figure S3). Gel-based activity assays were carried out to monitor the selection progress and enrichment of the DNA pools with Mn^{2+}-specific DNAzymes. High activity of the DNA pools from Round 11 was observed (Figure S4). Then, it was chosen for sequencing. After performing activity assays on the obtained sequences, one sequence with the highest selectivity was enriched and named 11-5 DNAzyme.

Sensitivity and Selectivity of 11-5 DNAzyme

The secondary structure of the cis-cleaving 11-5 DNAzyme was predicted by the UNAFold web package and is re-drawn in Figure 1A. We could see that part of the obtained 11-5

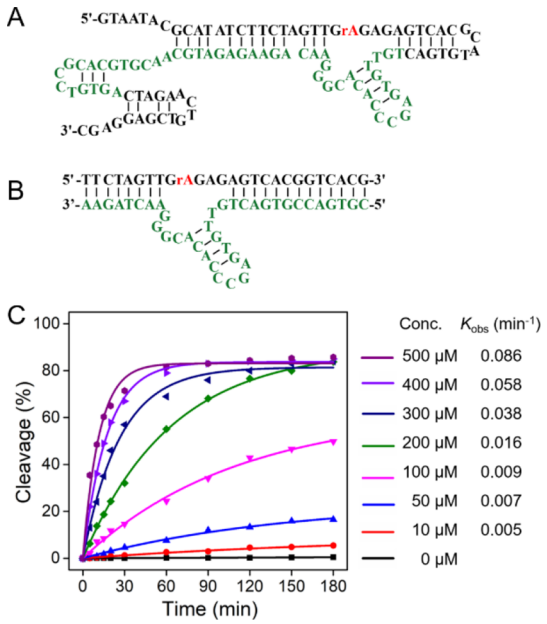

Figure 1. Sequences and activities of the in vitro selected Mn^{2+}-specific 11-5 DNAzyme. Secondary structure of 11-5 DNAzyme in its cis-cleaving form (A) and trans-cleaving form (B). (C) Activity of the trans-cleaving 11-5 DNAzyme in the presence of Mn^{2+} at different concentrations from a ^{32}P-radiolabeled PAGE assay.

DNAzyme is in the form of classic DNAzyme structure. Its activity to Mn^{2+} was first proved using GelRed-stained PAGE gels, and its RNA-cleaving feature was also confirmed (Figure S5). Then, we investigated its selectivity to Mn^{2+} over other metal ions. As shown in Figure S6, 14 competing metal ions were separately incubated with 11-5 DNAzyme for 2 h. They all exhibited negligible cleavage signals, suggesting its high selectivity for Mn^{2+}. We converted the 11-5 DNAzyme into the trans-cleaving structure through truncation and rational design of substrate binding sequences (Figure 1B). The strand that contains rA is the substrate, and the other strand is the enzyme. Activity of the trans-cleaving 11-5 DNAzyme was carried out in the presence of different concentrations of Mn^{2+} and quantified using a ^{32}P-radiolabeled PAGE assay (Figure 1C). Under 500 μM of Mn^{2+} in the selection buffer at room temperature, it displayed an initial observed rate constant ($k$obs) of 0.086 min^{-1}.

https://doi.org/10.1021/jacsau.3c00062
JACS Au 2023, 3, 1615−1622

11-5 DNAzyme-Based Fluorescent Sensor

To further evaluate the sensitivity of the trans-cleaving 11-5 DNAzyme for Mn^{2+} detection, we converted it into a turn-on fluorescent sensor through labeling the substrate strand with a Cy5 fluorophore at its 5′ end and labeling the enzyme strand with a BHQ2 quencher at its 3′ end. To minimize background fluorescence, a second BHQ2 quencher was additionally added at the 3′ end of the substrate strand. To form the sensor, the substrate and enzyme strands were mixed in the selection buffer and annealed by heating the solution to 95 °C in a water bath for 5 min followed by slowly cooling down to room temperature overnight. As a result, the fluorescence signal was greatly quenched owing to the close proximity of the fluorophore in the substrate strand and the quencher in the enzyme strand (Figure 2A). In the presence of Mn^{2+}, the

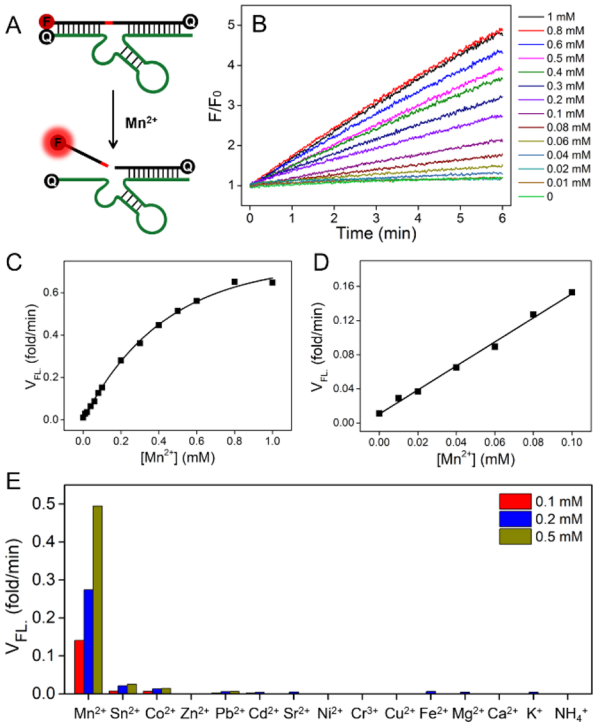

Figure 2. Design, activity, and selectivity of the 11-5 DNAzyme-based turn-on fluorescent sensor. (A) Schematic illustration of the sensor for Mn^{2+} detection. (B) Fluorescence enhancement of the sensor over time upon addition of different concentrations of Mn^{2+} in selection buffer. (C) Initial rate of fluorescence enhancement of the sensor in Figure B. (D) Linear response of the sensor at Mn^{2+} concentrations lower than 0.1 mM. (E) Response of the sensor to Mn^{2+} and different competing metal ions.

substrate strand was cleaved at the rA site, and the shorter arm labeled with the Cy5 fluorophore, which has a melting temperature (11.1 °C) below ambient temperature, was released, resulting in significant fluorescence recovery.

The prepared 11-5 DNAzyme-based fluorescent sensor was used to monitor the fluorescence increase over time in selection buffer with the addition of Mn^{2+} at different concentrations. As shown in Figure 2B, the fluorescence signal gradually increased with increasing concentrations of Mn^{2+}. The observed rate of fluorescence enhancement was accelerated with additional Mn^{2+}, until saturation at ∼1 mM Mn^{2+}. The dissociation constant (Kd) was 420 ± 12 μM (Figure 2C). A good linear relationship between them was observed with Mn^{2+} concentration lower than 100 μM (Figure 2D), which facilitated the detection of Mn^{2+} in biological systems, given that Mn^{2+} is in tens of micromolar range in living cells.[60] To further determine the selectivity of the 11-5 DNAzyme-based fluorescent sensor for Mn^{2+}, we monitored its response to other competing metal ions. As shown in Figures 2E and S7, compared with Mn^{2+}, all the competing metal ions exhibited negligible changes in the fluorescence signal, suggesting that the 11-5 DNAzyme-based fluorescent sensor has excellent selectivity for Mn^{2+}. The selectivities of 11-5 DNAzyme for Mn^{2+} at 0.1 mM against Ca^{2+}, Mg^{2+}, and Zn^{2+} was 480-, 174-, and 320- fold, respectively. Considering that Mg^{2+}, Ca^{2+}, and K^{+} are in high concentration under physiological conditions, we tested the fluorescence intensity of this sensor after incubation with metal ions in high concentration for 2 h. As shown in Figure S8, compared with 0.2 mM Mn^{2+}, 140 mM K^{+}, and 2 mM of other competing metal ions caused little fluorescence enhancement except that Pb^{2+} interfered a little. Given that lead is not an essential trace element for the human body,[61] it would not interfere with Mn^{2+} detection in cells. In addition, many DNAzymes have been reported to have Mn^{2+} dependency or use Mn^{2+} to facilitate high catalytic activity. Their selectivity for Mn^{2+} against other metal ions, however, is unsatisfactory. We compared the selectivity of 11-5 DNAzyme with the widely used 8-17 DNAzyme[40,41,63,64] and 10-23 DNAzyme,[37,38,62] which are also responsive to Mn^{2+}. Under the same condition with 11-5 DNAzyme, both 8-17E DNAzyme (Figure S9) and 10-23 DNAzyme (Figure S10) were responsive to Mn^{2+}, Pb^{2+}, Zn^{2+}, Mg^{2+}, and Cd^{2+}, exhibiting much poorer selectivity for Mn^{2+} against other metal ions. All these results indicated that 11-5 DNAzyme could be regarded as an ideal sensor for intracellular Mn^{2+} sensing.

Intracellular Delivery of 11-5 DNAzyme

To explore the application of this Mn^{2+}-specific DNAzyme in intracellular sensing of Mn^{2+}, we used lipofectamine 3000, a commercial transfection reagent for DNA and siRNA, to deliver the DNAzyme-based fluorescent sensor into living cells. To visualize the internalization of the sensor, only the Cy5-labeled sensor without quenchers was delivered into human breast carcinoma cells (MCF-7). As shown in Figure 3A, after

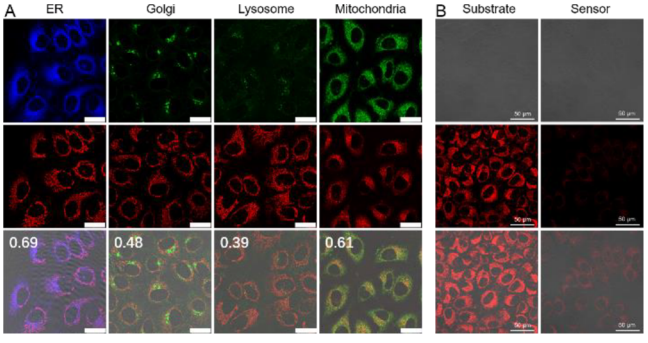

Figure 3. Intracellular delivery of the 11-5 DNAzyme-based fluorescent sensor into MCF-7 cells by lipofectamine 3000. (A) Internalization of the Cy5-labeled sensor without quenchers and its co-localization with ER-tracker, Golgi-tracker, lysosome-tracker, and mitochondria-tracker. Numbers inside were Pearson's correlation coefficient (PCC) (scale bar: 20 μm). (B) Confocal images of MCF-7 cells transfected with the Cy5-labeled substrate and Cy5/BHQ2-labeled sensor.

https://doi.org/10.1021/jacsau.3c00062
JACS Au 2023, 3, 1615−1622

5 h incubation, high delivery efficiency of the DNAzyme sensor into the cytoplasm was achieved. To further confirm localization of the sensor inside cells, we stained the cells with subcellular organelle trackers. It could be seen that Cy5-labeled sensor overlapped well with ER-tracker (PCC = 0.69) and mitochondria-tracker (PCC = 0.61), but did not co-localize well with Golgi-tracker (PCC = 0.48) and lysosome-tracker (PCC = 0.39), suggesting that the sensor was mainly located in the cytosol and mitochondria. It is frequently reported that Mn^{2+} is enriched in mitochondria,[65] indicating the high applicability of this sensor to intracellular Mn^{2+} detection. Moreover, to investigate the stability of this sensor during the transfection process, we delivered only the Cy5-labled substrate and Cy5/BHQ2-labled DNAzyme sensor into MCF-7 cells. As shown in Figure 3B, compared with the Cy5-labeled substrate, the DNAzyme sensor showed minimal background fluorescence after 5 h delivery, ruling out nonspecific degradation or activation of the sensor during the delivery process.

Intracellular Mn^{2+} Imaging Using 11-5 DNAzyme

Next, we used the 11-5 DNAzyme-based fluorescent sensor to detect Mn^{2+} in MCF-7 cells. To use a mutant DNAzyme as a control, we included a site-specific mutation of residues in the single-stranded region of 11-5 DNAzyme, which resulted in negligible activity and selectivity (Figure S11). We then compared the activities of 11-5 DNAzyme, the mutant DNAzyme, and negative control (containing a noncleavable substrate) in selection buffer. As shown in Figures S12 and S13, neither mutant DNAzyme nor negative control responded to Mn^{2+} even at high concentration. Toxicity assay indicated that MCF-7 cells could tolerate up to 3 mM Mn^{2+} treatment in 5 h (Figure S14). Thus, MCF-7 cells were transfected with fluorescent sensors and then incubated with Mn^{2+} below 3 mM. As shown in Figure 4A, with the increase of Mn^{2+}

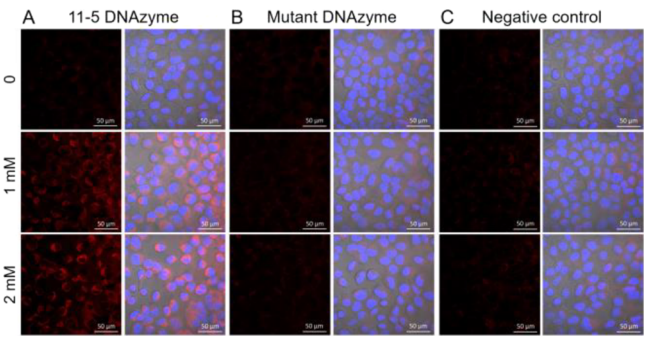

Figure 4. Intracellular imaging of Mn^{2+} using DNAzyme-based fluorescent sensors. Confocal images of MCF-7 cells transfected with 11-5 DNAzyme (A), mutant DNAzyme (B), and negative control (C) upon addition of different concentrations of $MnCl_2$.

concentration, the fluorescence signal in 11-5 DNAzyme-treated cells gradually increased. In comparison, the mutant DNAzyme (Figure 4B) and negative control (Figure 4C) displayed no fluorescence increase inside the cells. We further applied the active sensor to MCF-7 cells treated with different concentrations of Zn^{2+}. No fluorescence signal was observed until Zn^{2+} concentration became toxic to MCF-7 (Figure S15). In addition, Mn^{2+} has been discovered to be essential for cGAS-STING activation in innate immunity.[5,6] Its detection in immune cells would provide an opportunity for discovering more functions of Mn^{2+} in the immune response. cGAS-STING activation triggered by Mn^{2+} in human acute monocytic leukemia cells (THP-1) was first demonstrated (Figure S16). Then, THP-1 cells were transfected with the 11-5 DNAzyme-based fluorescent sensor and treated with different concentrations of Mn^{2+}. As shown in Figure S17, a gradually increased fluorescence signal was observed with the increase of Mn^{2+} concentration in the range of cGAS-STING activation. All these results confirmed the ability of the 11-5 DNAzyme-based fluorescent sensor to sense Mn^{2+} in tumor cells and immune cells.

MnOx nanoparticles are becoming popular nanocarriers or nanoadjuvants for antitumor therapy in recent years.[66−68] In most cases, MnOx need to degrade into Mn^{2+} in the tumor microenvironment to perform their function and enhance the treatment effect. Therefore, a Mn^{2+}-specific sensor would allow monitoring the degradation and distribution of the MnOx nanoparticles in living organisms, providing information on drug release and therapeutic response. To achieve this goal, we synthesized MnOx nanoparticles in a protocol reported previously[66] and characterized their morphology using scanning electron microscopy (SEM) (Figure S18). MCF-7 cells were transfected with the 11-5 DNAzyme-based fluorescent sensor and then incubated with different concentrations of MnOx nanoparticles. As shown in Figure 5A, an obvious fluorescence signal was observed with 11-5

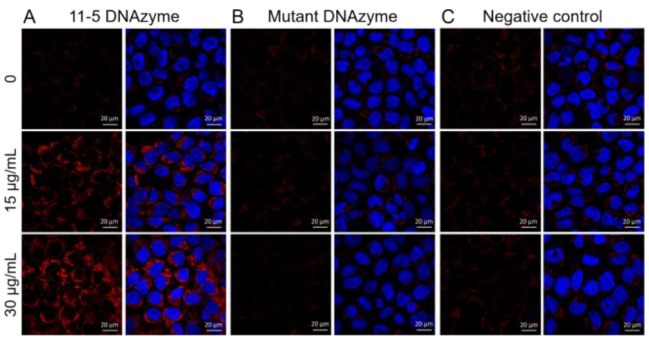

Figure 5. Intracellular imaging of MnOx nanoparticles using DNAzyme-based fluorescent sensors. Confocal images of MCF-7 cells transfected with 11-5 DNAzyme (A), mutant DNAzyme (B), and negative control (C) upon incubation with different concentrations of MnOx nanoparticles.

DNAzyme treatment and MnOx addition, indicating that MnOx nanoparticles were taken up by MCF-7 cells and degraded into Mn^{2+} inside the cells. In comparison, the mutant DNAzyme (Figure 5B) and negative control (Figure 5C) exhibited a negligible fluorescent signal inside the cells. All these results indicated that the 11-5 DNAzyme-based fluorescent sensor had great potential to monitor the degradation of manganese-based nanomaterials in vivo and provided the opportunity for imaging-guided antitumor therapy.

CONCLUSIONS

In conclusion, we have selected a Mn^{2+}-specific RNA-cleaving DNAzyme, named 11-5, which exhibited exceptionally high selectivity for Mn^{2+} over other competing metal ions, especially Ca^{2+}, Mg^{2+}, and Zn^{2+} which are similar to Mn^{2+} and abundant in cells. Taking advantage of this selectivity, we converted it into a fluorescent turn-on sensor based on the catalytic beacon approach. Separation of the metal-binding site and fluorophore

https://doi.org/10.1021/jacsau.3c00062
JACS Au 2023, 3, 1615−1622

avoided the fluorescence quenching by Mn^{2+}. By using lipofectamine 3000 as the delivery method, the 11-5 DNAzyme-based fluorescent sensor was efficiently delivered into cells and achieved Mn^{2+} sensing in immune cells and tumor cells. Degradation of manganese-based nanomaterials such as MnOx in tumor cells was also observed. Therefore, the selected 11-5 DNAzyme has great potential to detect Mn^{2+} in the biological systems and provides an excellent tool to monitor the Mn^{2+}-involved immune response and antitumor therapy.

METHODS

Materials

Metal salts used were NaCl (Alfa Aesar, 99.999%), KCl (Alfa Aesar 99.999%), $Mn(CH_3CO_2)_2{\cdot}4H_2O$ (Alfa Aesar, 99.999%), $MnCl_2{\cdot}4H_2O$ (Sigma, 99.99%), $ZnCl_2{\cdot}H_2O$ (Alfa Aesar, 99.99%), $Pb(CH_3CO_2)_2{\cdot}3H_2O$ (Aldrich, 99.999%), $MgCl_2{\cdot}6H_2O$ (Alfa Aesar, 99.999%), $Ca(NO_3)_2{\cdot}6H_2O$ (Alfa Aesar, 99.995%), $FeCl_2$ (Alfa Aesar, 99.99%), $CdCl_2$ (Sigma, 99.99%), $SrCl_2$ (Alfa Aesar 99.999%), $CoCl_2$ (Alfa Aesar 99.999%), $SnCl_2{\cdot}2H_2O$ (Alfa Aesar 99.99%), $NiCl_2$ (Alfa Aesar 99.99%), $CrCl_3$ (Sigma, 99.0%), and $CuCl_2{\cdot}2H_2O$ (Alfa Aesar 99.99%). Other chemicals used to prepare different solutions were EDTA·2Na·$2H_2O$ (Fisher Scientific), urea (Affymetrix, MB grade), Tris (Affymetrix, MB grade), and boric acid (Fisher Scientific, electrophoresis grade). Acrylamide/bisacrylamide 40% solution (29:1) was obtained from Bio-Rad Laboratories, Inc. T4-polynucleotide kinase, Taq DNA polymerase, and deoxynucleotide (dNTP) solution mix were obtained from New England Biolabs. ^{32}P labeled α-ATP and γ-ATP for DNA radiolabeling were obtained from PerkinElmer. α-ATP worked the same as dATP at a much higher concentration, and it was embedded into DNA. γ-ATP was labeled on the 5′ end of DNA. One molecule of DNA was labeled with one molecule of γ-ATP. All PCR and ^{32}P-labeling experiments were carried out in the Bio-Rad thermocycler. The selection buffer was made as a 10× solution of 50 mM Bis-Tris (Sigma, 99.0%) containing 300 mM sodium chloride (Alfa Aesar, 99.999%) at pH 6.8. 100 mM manganese acetate was prepared fresh every time as Mn(II) metal-stock solution for positive selection. NaOH (Alfa Aesar, 99.996%) and HCl (Alfa Aesar, 36.5%) were used to adjust pH of buffer solutions with a Fisher Scientific Accumet AB15 pH meter. All buffer and gel stock solutions were prepared with a Milli-Q water purification system (Billerica, MA, USA) with an electrical resistance >18.3 MΩ.

In Vitro Selection

The in vitro selection method was originally reported by Breaker and Joyce in combination with the denaturing PAGE-based separation method. The initial random pool was generated using the PCR machine (C1000 Touch Thermal Cycler from Bio-Rad Laboratories, Inc). 0.1 μM counter template and 1 μM rP-rA primer were mixed with the PCR mixture containing 0.2 mM dNTPs, 6 U/100 μL Taq. and 3 μL of [α-^{32}P]-dATP in a volume of 3 mL and subsequently divided into 96 PCR tubes. After 17 cycles of extension, the generated PCR products were precipitated by adding 10% of a 3 M sodium acetate solution (pH 5.2) and 2.7 × volume of cold ethanol. The samples were then stored at −80 °C overnight. Finally, the DNA samples were centrifuged, washed, and lyophilized.

Dried DNA samples were dissolved in deionized water. To purify the DNA pool, a 10% denaturing PAGE gel was used with 1 × TBE (Tris, Boric acid, EDTA) as the running buffer. The DNA pool was mixed with an equal amount of stop buffer (50 mM EDTA, 8 M urea, 0.05% xylene cyanol, 0.05% bromophenol blue, 1 × TBE) and subjected to the PAGE gel purification. Radioactive DNA size markers corresponding to the cleaved (87-mer) and intact (110-mer) pool were added alongside. After electrophoresis, the gel was taken out and covered with a plastic wrap. Then radioactive location markers were placed on top of the gel and exposed to a phosphorimager cassette for about 15 min. The exposed film was imaged on a Molecular Dynamics Storm 430 Phosphorimager (Amersham Biosciences). The DNA band corresponds to the 110-mer marker on the gel was excised, crushed in a centrifuge tube, and extracted with an extraction buffer containing 10 mM Tris, 0.1 mM EDTA, and 300 mM sodium chloride. Gel particles in the extraction buffer were frozen at −80 °C over 10 min and then thawed in a room-temperature water bath over 5 min to improve extraction efficiency. The solution was centrifuged to acquire gel free solution containing DNA. DNA samples were finally ethanol precipitated.

The dried pool after the initial pool generation was dissolved in 1 × selection buffer and incubated for 2 h without addition of any divalent metal ions as the initial negative selection for the first selection round. After the negative step, uncleaved DNA pools were PAGE-purified and subjected to the subsequent positive selection which was carried out by incubating the DNA pool with 500 μM manganese acetate for 2 h. After the positive step, cleaved DNA pools were PAGE-purified and used as a template for PCR amplification reactions. Two steps of PCR reactions were needed to regenerate selection pools. PCR1 was performed to convert the cleaved DNA sequence into the initial counter template. PCR2 was performed to convert the counter template into the rA-containing pool for the next round selection.

From R1 to R7, negative selections were carried out by incubating the DNA pools in the selection buffer for 2 h without addition of any divalent metal ions. From R8 to R11, negative selections were replaced by counter selections which were performed by incubating the DNA pools in the selection buffer with addition of 0.5 mM Zn^{2+}, 0.5 mM Cu^{2+}, 0.1 mM Pb^{2+}, 10 mM Mg^{2+}, and 10 mM Ca^{2+} for 2 h. Positive selections in the whole selection process were carried out by treating the DNA pools with 0.5 mM Mn^{2+} in the selection buffer, and the reaction time was gradually shortened to increase the stringency of positive selections to search for more efficient DNAzymes. All selection reactions were stopped by adding an equal amount of stop buffer. All amplification reactions were carried out by PCR. All PAGE purifications were carried out using 10% PAGE gels.

Eleventh round pool was submitted to Sangon Biotechnology (Shanghai, China) for next-generation sequencing (NGS). We analyzed the obtained sequences with an abundance ratio bigger than 1% (top16) and tested the activity and selectivity of those in classic DNAzyme structure to find the best Mn^{2+}-specific DNAzymes.

Gel-Based Activity Assays

In order to monitor the enhancement of DNA pools with Mn^{2+}-specific DNAzymes in the selection process, gel-based activity assays were performed after the third round of the selection. Single-stranded DNA pools from each round selection were PCR amplified and internally labeled with ^{32}P. After PAGE purification, the PCR products were dissolved in selection buffer and incubated with Mn^{2+} or other competing metal ions. Each reaction was initiated by adding an equal volume of 2 × metal solution into the DNA pool in 2 × selection buffer. At known time points, an equal amount of stop buffer was added. Finally, the cleaved and uncleaved DNA pools were separated on a 10% PAGE gel and imaged using a Molecular Dynamics Storm 430 Phosphorimager (Amersham Biosciences). The fraction of cleavage was calculated using Image Quant software (Molecular Dynamics).

^{32}P-labeled *cis*-cleaving 11-5 DNAzyme was used to detect its activities to Mn^{2+} in the way mentioned above. Its selectivity to different manganese salts or different metal ions was carried out in a different way. 1 μL of concentrated Mn^{2+} or other metal ions were added into 9 μL of cis-cleaving 11-5 DNAzyme (1 μM), and the mixture was incubated at room temperature. After 2 h incubation, 2 μL of 6 × loading buffer containing 30 mM EDTA, 36% glycerol, 0.035% xylene cyanol, and 0.05% bromophenol blue (Takara, China) was added. The cleaved DNA strands were separated on a 12% PAGE gel. The gel was then stained with GelRed (Biotium) and imaged as well as analyzed using a Bio-Rad ChemiDoc XRS+ System.

https://doi.org/10.1021/jacsau.3c00062
JACS Au 2023, 3, 1615−1622

Preparation of the Fluorescent Sensor and Mn^{2+} Detection in Selection Buffer

The BHQ2-labeled enzyme strand and Cy5 as well as BHQ2-labeled substrate strand were mixed with a ratio of 1.2:1 in selection buffer. The mixture was annealed by heating the solution to 95 °C in a water bath for 5 min followed by slowly cooling down to room temperature overnight, to form the fluorescent sensor with a final concentration of 100 nM. Concentrated Mn^{2+} or other metal solutions were quickly mixed with the prepared sensor, and the fluorescence change was continuously monitored on a fluoromax-4 spectrofluorometer (HORIBA JobinYvon, Edison, NJ) with an excitation wavelength of 630 nm and an emission wavelength of 631 nm. The initial rate of fluorescence enhancement was measured by using a linear fit to plot the change in fluorescence intensity for the first 6 min after Mn^{2+} addition. Selectivity of the fluorescent sensor for Mn^{2+} was studied by recording its fluorescence changes upon addition of different metal ions (Mn^{2+}, Mg^{2+}, Ca^{2+}, Sr^{2+}, Sn^{2+}, Co^{2+}, Ni^{2+}, Cu^{2+}, Zn^{2+}, Cd^{2+}, Fe^{2+}, Pb^{2+}, Cr^{3+}, K^{+}, and NH_4^{+}) at different concentrations.

Preparation of the Intracellular Fluorescent Sensor

The 11-5 enzyme strand labeled with BHQ2 (Enzyme-BHQ2) was mixed with the substrate strand labeled with Cy5 and BHQ2 (Cy5-Substrate-BHQ2) with a ratio of 1.5−1.0 in selection buffer. The two DNA strands were then annealed by heating the solution to 95 °C in a water bath for 5 min followed by slowly cooling down to room temperature overnight to form the 11-5 DNAzyme-based fluorescent sensor for cell imaging.

Preparation and Characterization of MnOx Nanoparticles

0.2 g of $KMnO_4$ was dissolved in 100 mL of distilled water, and the solution was fleetly stirred at room temperature for about 0.5 h. Two milliliters of oleic acid (90%) was then added. The resulting mixture was reacted at room temperature for 10 h. A crude brown-black product was finally collected. The product was centrifuged and washed several times with deionized water and alcohol to remove any possible residual reactants. SEM (SU8100) was used to characterize the morphology of the prepared MnOx nanoparticles.

Fluorescent Sensor Delivery and Colocalization Study

For the delivery of DNAzyme-based fluorescent sensors, we used lipofectamine 3000 (Invitrogen by Thermo Fisher Scientific) as the transfection reagent. 2×10^5 MCF-7 cells were seeded in a 35 mm confocal dish and incubated for another 24 h to be 70−90% confluent. 5.5 μL of lipofectamine 3000 was diluted into 250 μL of Opti-MEM (Gbico). Annealed DNAzyme sensors were also diluted into 250 μL of Opti-MEM. Then diluted lipofectamine 3000 and DNAzyme sensors were mixed (1:1 ratio) and incubated at room temperature for 10−15 min. Finally, half of the mixture was mixed with 750 μL of cell media and incubated with cells for 5 h.

After incubating MCF-7 cells with DNAzyme sensors for 5 h, cells were washed thoroughly with D-PBS three times. Delivered DNAzyme sensors were labeled with Cy5 (648−750 nm, λ_{ex} 633 nm). Subcellular organelles inside cells were stained with commercial dyes, such as ER-Blue (428−630 nm, λ_{ex} 405 nm), Golgi-Green (492−555 nm, λ_{ex} 488 nm), Lyso-Green (492−630 nm, λ_{ex} 488 nm), and Miti-Green (492−555 nm, λ_{ex} 488 nm). Images were obtained on a confocal microscope (ZEISS LSM 710). The pinhole and gain settings were kept constant throughout the whole imaging process.

Fluorescence Imaging of Intracellular Mn^{2+}

2×10^5 MCF-7 cells were seeded in a 35 mm confocal dish and incubated for another 24 h. After washing with D-PBS, cells were transfected with 250 nM 11-5 DNAzyme, mutant DNAzyme, or negative control-based fluorescent sensor using lipofectamine 3000 reagent. After 5 h incubation, the culture medium was discarded, and the cells were washed thoroughly with D-PBS to remove excess sensors. Then the cells were further incubated with different concentrations of $MnCl_2$ or MnOx nanoparticles in 1 mL of culture medium. After 4 h incubation, cells were washed with D-PBS and subjected to confocal microscope imaging (ZEISS LSM 710).

ASSOCIATED CONTENT

Supporting Information

The Supporting Information is available free of charge at https://pubs.acs.org/doi/10.1021/jacsau.3c00062.

DNA sequences, additional methods, and supplementary figures as mentioned in the text (PDF)

AUTHOR INFORMATION

Corresponding Authors

Huanhuan Fan − *State Key Laboratory of Coordination Chemistry, School of Chemistry and Chemical Engineering, Chemistry and Biomedicine Innovation Center (ChemBIC), Nanjing University, Nanjing 210023, China;* orcid.org/0000-0002-5779-5786; Email: fanhh911@nju.edu.cn

Xiao-Bing Zhang − *Molecular Science and Biomedicine Laboratory, State Key Laboratory of Chemo/Bio-Sensing and Chemometrics, College of Chemistry and Chemical Engineering, Collaborative Innovation Center for Chemistry and Molecular Medicine, Hunan University, Changsha 410082, China;* orcid.org/0000-0002-4010-0028; Email: xbzhang@hnu.edu.cn

Yi Lu − *Department of Chemistry, University of Illinois at Urbana-Champaign, Urbana, Illinois 61801, United States;* orcid.org/0000-0003-1221-6709; Email: yi-lu@illinois.edu

Authors

Claire E. McGhee − *Department of Chemistry, University of Illinois at Urbana-Champaign, Urbana, Illinois 61801, United States*

Ryan J. Lake − *Department of Chemistry, University of Illinois at Urbana-Champaign, Urbana, Illinois 61801, United States*

Zhenglin Yang − *Department of Chemistry, University of Illinois at Urbana-Champaign, Urbana, Illinois 61801, United States*

Zijian Guo − *State Key Laboratory of Coordination Chemistry, School of Chemistry and Chemical Engineering, Chemistry and Biomedicine Innovation Center (ChemBIC), Nanjing University, Nanjing 210023, China;* orcid.org/0000-0003-4986-9308

Complete contact information is available at: https://pubs.acs.org/10.1021/jacsau.3c00062

Author Contributions

H.F. performed the experiments and analyzed the results. C.E.M., R.J.L., and Z.Y. helped data analyses. H.F. drew the figures and wrote the manuscript. X.Z. and Y.L. finalized the manuscript and supervised this project. H.F., Z.G., and Y.L. provided funding. CRediT: **Huanhuan Fan** data curation, formal analysis, funding acquisition, writing-original draft; **Claire E. McGhee** data curation, formal analysis; **Ryan J. Lake** formal analysis, writing-review & editing; **Zhenglin Yang** data curation, formal analysis, writing-review & editing; **Zijian Guo** formal analysis, funding acquisition; **Xiao-Bing Zhang** supervision; **Yi Lu** data curation, formal analysis, funding acquisition, supervision, writing-review & editing.

Notes

The authors declare no competing financial interest.

https://doi.org/10.1021/jacsau.3c00062
JACS Au 2023, 3, 1615−1622

■ ACKNOWLEDGMENTS

This work was financially supported by the National Natural Science Foundation of China (22107049 to H.F. and 92153303 to Z.G.), the Natural Science Foundation of Jiangsu Province (BK20202004 to Z.G.), and US National Institute of Health (GM141931 to Y.L.).

■ REFERENCES

(1) Aschner, M.; Erikson, K. Manganese. *Adv. Nutr.* **2017**, *8*, 520−521.
(2) Law, N. A.; Caudle, M. T.; Pecoraro, V. L. Manganese Redox Enzymes and Model Systems: Properties, Structures, and Reactivity. *Adv. Inorg. Chem.* **1998**, *46*, 305−440.
(3) Paynter, D. I. Changes in Activity of the Manganese Superoxide Dismutase Enzyme in Tissues of the Rat with Changes in Dietary Manganese. *J. Nutr.* **1980**, *110*, 437−447.
(4) Li, W.; Liu, Z.; Liu, C.; Guan, Y.; Ren, J.; Qu, X. Manganese Dioxide Nanozymes as Responsive Cytoprotective Shells for Individual Living Cell Encapsulation. *Angew. Chem., Int. Ed.* **2017**, *56*, 13661−13665.
(5) Wang, C.; Guan, Y.; Lv, M.; Zhang, R.; Guo, Z.; Wei, X.; Du, X.; Yang, J.; Li, T.; Wan, Y.; Su, X.; Huang, X.; Jiang, Z. Manganese Increases the Sensitivity of the cGAS-STING Pathway for Double-Stranded DNA and Is Required for the Host Defense against DNA Viruses. *Immunity* **2018**, *48*, 675−687.e7.
(6) Zhao, Z.; Ma, Z.; Wang, B.; Guan, Y.; Su, X. D.; Jiang, Z. Mn^{2+} Directly Activates cGAS and Structural Analysis Suggests Mn^{2+} Induces a Noncanonical Catalytic Synthesis of 2′3′-cGAMP. *Cell Rep.* **2020**, *32*, No. 108053.
(7) Ding, B.; Zheng, P.; Ma, P.; Lin, J. Manganese Oxide Nanomaterials: Synthesis, Properties, and Theranostic Applications. *Adv. Mater.* **2020**, *32*, No. 1905823.
(8) Zhang, Z.; Ji, Y. Nanostructured Manganese Dioxide for Anticancer Applications: Preparation, Diagnosis, and Therapy. *Nanoscale* **2020**, *12*, 17982−18003.
(9) Lv, M.; Chen, M.; Zhang, R.; Zhang, W.; Wang, C.; Zhang, Y.; Wei, X.; Guan, Y.; Liu, J.; Feng, K.; Jing, M.; Wang, X.; Liu, Y. C.; Mei, Q.; Han, W.; Jiang, Z. Manganese Is Critical for Antitumor Immune Responses via cGAS-STING and Improves the Efficacy of Clinical Immunotherapy. *Cell Res.* **2020**, *30*, 966−979.
(10) Sun, X.; Zhang, Y.; Li, J.; Park, K. S.; Han, K.; Zhou, X.; Xu, Y.; Nam, J.; Xu, J.; Shi, X.; Wei, L.; Lei, Y. L.; Moon, J. J. Amplifying STING Activation by Cyclic Dinucleotide-Manganese Particles for Local and Systemic Cancer Metalloimmunotherapy. *Nat. Nanotechnol.* **2021**, *16*, 1260−1270.
(11) Roels, H. A.; Bowler, R. M.; Kim, Y.; Claus Henn, B.; Mergler, D.; Hoet, P.; Gocheva, V. V.; Bellinger, D. C.; Wright, R. O.; Harris, M. G.; Chang, Y.; Bouchard, M. F.; Riojas-Rodriguez, H.; Menezes-Filho, J. A.; Téllez-Rojo, M. M. Manganese Exposure and Cognitive Deficits: A Growing Concern for Manganese Neurotoxicity. *Neurotoxicology* **2012**, *33*, 872−880.
(12) Cao, X.; Sun, Y.; Lu, P.; Zhao, M. Fluorescence Imaging of Intracellular Nucleases-A Review. *Anal. Chim. Acta* **2020**, *1137*, 225−237.
(13) Ji, Y.; Jones, C.; Baek, Y.; Park, G. K.; Kashiwagi, S.; Choi, H. S. Near-Infrared Fluorescence Imaging in Immunotherapy. *Adv. Drug Delivery Rev.* **2020**, *167*, 121−134.
(14) Hoi, H.; Matsuda, T.; Nagai, T.; Campbell, R. E. Highlightable Ca^{2+} Indicators for Live Cell Imaging. *J. Am. Chem. Soc.* **2013**, *135*, 46−49.
(15) Komatsu, H.; Miki, T.; Citterio, D.; Kubota, T.; Shindo, Y.; Kitamura, Y.; Oka, K.; Suzuki, K. Single Molecular Multianalyte (Ca^{2+}, Mg^{2+}) Fluorescent Probe and Applications to Bioimaging. *J. Am. Chem. Soc.* **2005**, *127*, 10798−10799.
(16) Komatsu, H.; Iwasawa, N.; Citterio, D.; Suzuki, Y.; Kubota, T.; Tokuno, K.; Kitamura, Y.; Oka, K.; Suzuki, K. Design and Synthesis of Highly Sensitive and Selective Fluorescein-Derived Magnesium Fluorescent Probes and Application to Intracellular 3D Mg^{2+} Imaging. *J. Am. Chem. Soc.* **2004**, *126*, 16353−16360.
(17) Farruggia, G.; Iotti, S.; Prodi, L.; Montalti, M.; Zaccheroni, N.; Savage, P. B.; Trapani, V.; Sale, P.; Wolf, F. I. 8-Hydroxyquinoline Derivatives as Fluorescent Sensors for Magnesium in Living Cells. *J. Am. Chem. Soc.* **2006**, *128*, 344−350.
(18) Kim, H. M.; Jung, C.; Kim, B. R.; Jung, S. Y.; Hong, J. H.; Ko, Y. G.; Lee, K. J.; Cho, B. R. Environment-Sensitive Two-Photon Probe for Intracellular Free Magnesium Ions in Live Tissue. *Angew. Chem., Int. Ed.* **2007**, *46*, 3460−3463.
(19) Qian, F.; Zhang, C.; Zhang, Y.; He, W.; Gao, X.; Hu, P.; Guo, Z. Visible Light Excitable Zn^{2+} Fluorescent Sensor Derived from an Intramolecular Charge Transfer Fluorophore and Its in Vitro and in Vivo Application. *J. Am. Chem. Soc.* **2009**, *131*, 1460−1468.
(20) Fang, H.; Geng, S.; Hao, M.; Chen, Q.; Liu, M.; Liu, C.; Tian, Z.; Wang, C.; Takebe, T.; Guan, J. L.; Chen, Y.; Guo, Z.; He, W.; Diao, J. Simultaneous Zn^{2+} Tracking in Multiple Organelles Using Super-Resolution Morphology-Correlated Organelle Identification in Living Cells. *Nat. Commun.* **2021**, *12*, 109.
(21) Chen, Y.; Bai, Y.; Han, Z.; He, W.; Guo, Z. Photoluminescence Imaging of Zn^{2+} in Living Systems. *Chem. Soc. Rev.* **2015**, *44*, 4517−4546.
(22) Taki, M.; Iyoshi, S.; Ojida, A.; Hamachi, I.; Yamamoto, Y. Development of Highly Sensitive Fluorescent Probes for Detection of Intracellular Copper(I) in Living Systems. *J. Am. Chem. Soc.* **2010**, *132*, 5938−5939.
(23) Xu, H.; Yao, S.; Chen, Y.; Zhang, C.; Zhang, S.; Yuan, H.; Chen, Z.; Bai, Y.; Yang, T.; Guo, Z.; He, W. Tracking Labile Copper Fluctuation in Vivo/ex Vivo: Design and Application of a Ratiometric Near-Infrared Fluorophore Derived from 4-Aminostyrene-Conjugated Boron Dipyrromethene. *Inorg. Chem.* **2021**, *60*, 18567−18574.
(24) Cotruvo, J. A., Jr.; Aron, A. T.; Ramos-Torres, K. M.; Chang, C. J. Synthetic Fluorescent Probes for Studying Copper in Biological Systems. *Chem. Soc. Rev.* **2015**, *44*, 4400−4414.
(25) Gao, J.; He, Y.; Chen, Y.; Song, D.; Zhang, Y.; Qi, F.; Guo, Z.; He, W. Reversible FRET Fluorescent Probe for Ratiometric Tracking of Endogenous Fe^{3+} in Ferroptosis. *Inorg. Chem.* **2020**, *59*, 10920−10927.
(26) Kasha, M. Collisional Perturbation of Spin-Orbital Coupling and the Mechanism of Fluorescence Quenching. A Visual Demonstration of the Perturbation. *J. Chem. Phys.* **1952**, *20*, 71−74.
(27) McGlynn, S. P.; Azumi, T.; Kasha, M. External Heavy-Atom Spin-Orbital Coupling Effect. V. Absorption Studies of Triplet States. *J. Chem. Phys.* **1964**, *40*, 507−515.
(28) Park, J.; Cleary, M. B.; Li, D.; Mattocks, J. A.; Xu, J.; Wang, H.; Mukhopadhyay, S.; Gale, E. M.; Cotruvo, J. A., Jr. A Genetically Encoded Fluorescent Sensor for Manganese(II), Engineered from Lanmodulin. *Proc. Natl. Acad. Sci. U. S. A.* **2022**, *119*, No. e2212723119.
(29) Miyawaki, A.; Llopis, J.; Heim, R.; McCaffery, J. M.; Adams, J. A.; Ikura, M.; Tsien, R. Y. Fluorescent Indicators for Ca^{2+} Based on Green Fluorescent Proteins and Calmodulin. *Nature* **1997**, *388*, 882−887.
(30) Romani, A. M. Cellular Magnesium Homeostasis. *Arch. Biochem. Biophys.* **2011**, *512*, 1−23.
(31) Li, Y.; Breaker, R. R. Deoxyribozymes: New Players in the Ancient Game of Biocatalysis. *Curr. Opin. Struct. Biol.* **1999**, *9*, 315−323.
(32) Wang, D. Y.; Lai, B. H.; Sen, D. A General Strategy for Effector-Mediated Control of RNA-Cleaving Ribozymes and DNA Enzymes. *J. Mol. Biol.* **2002**, *318*, 33−43.
(33) Wang, D. Y.; Lai, B. H.; Feldman, A. R.; Sen, D. A General Approach for the Use of Oligonucleotide Effectors to Regulate the Catalysis of RNA-Cleaving Ribozymes and DNAzymes. *Nucleic Acids Res.* **2002**, *30*, 1735−1742.
(34) Breaker, R. R.; Joyce, G. F. A DNA Enzyme that Cleaves RNA. *Chem. Biol.* **1994**, *1*, 223−229.
(35) Liu, J.; Brown, A. K.; Meng, X.; Cropek, D. M.; Istok, J. D.; Watson, D. B.; Lu, Y. A Catalytic Beacon Sensor for Uranium with

https://doi.org/10.1021/jacsau.3c00062
JACS Au 2023, 3, 1615−1622

Parts-per-trillion Sensitivity and Millionfold Selectivity. *Proc. Natl. Acad. Sci. U. S. A.* **2007**, *104*, 2056−2061.
(36) Wu, P.; Hwang, K.; Lan, T.; Lu, Y. A DNAzyme-Gold Nanoparticle Probe for Uranyl Ion in Living Cells. *J. Am. Chem. Soc.* **2013**, *135*, 5254−5257.
(37) Hwang, K.; Wu, P.; Kim, T.; Lei, L.; Tian, S.; Wang, Y.; Lu, Y. Photocaged DNAzymes as a General Method for Sensing Metal Ions in Living Cells. *Angew. Chem., Int. Ed.* **2014**, *53*, 13798−13802.
(38) Lu, L. M.; Zhang, X. B.; Kong, R. M.; Yang, B.; Tan, W. A Ligation-Triggered DNAzyme Cascade for Amplified Fluorescence Detection of Biological Small Molecules with Zero-Background Signal. *J. Am. Chem. Soc.* **2011**, *133*, 11686−11691.
(39) Li, J.; Lu, Y. A Highly Sensitive and Selective Catalytic DNA Biosensor for Lead Ions. *J. Am. Chem. Soc.* **2000**, *122*, 10466−10467.
(40) Santoro, S. W.; Joyce, G. F. A General Purpose RNA-Cleaving DNA Enzyme. *Proc. Natl. Acad. Sci. U. S. A.* **1997**, *94*, 4262−4266.
(41) Qiu, L.; Zhang, T.; Jiang, J.; Wu, C.; Zhu, G.; You, M.; Chen, X.; Zhang, L.; Cui, C.; Yu, R.; Tan, W. Cell Membrane-Anchored Biosensors for Real-Time Monitoring of the Cellular Microenvironment. *J. Am. Chem. Soc.* **2014**, *136*, 13090−13093.
(42) Nelson, K. E.; Ihms, H. E.; Mazumdar, D.; Bruesehoff, P. J.; Lu, Y. The Importance of Peripheral Sequences in Determining the Metal Selectivity of an in Vitro-Selected Co^{2+}-Dependent DNAzyme. *ChemBioChem* **2012**, *13*, 381−391.
(43) Huang, P. J.; Liu, J. An Ultrasensitive Light-up Cu^{2+} Biosensor Using a New DNAzyme Cleaving a Phosphorothioate-Modified Substrate. *Anal. Chem.* **2016**, *88*, 3341−3347.
(44) Huang, P. J.; Liu, J. Rational Evolution of Cd^{2+}-Specific DNAzymes with Phosphorothioate Modified Cleavage Junction and Cd^{2+} Sensing. *Nucleic Acids Res.* **2015**, *43*, 6125−6133.
(45) Liu, J.; Lu, Y. Rational Design of "Turn-on" Allosteric DNAzyme Catalytic Beacons for Aqueous Mercury Ions with Ultrahigh Sensitivity and Selectivity. *Angew. Chem., Int. Ed.* **2007**, *46*, 7587−7590.
(46) Saran, R.; Liu, J. A Silver DNAzyme. *Anal. Chem.* **2016**, *88*, 4014−4020.
(47) Torabi, S. F.; Wu, P.; McGhee, C. E.; Chen, L.; Hwang, K.; Zheng, N.; Cheng, J.; Lu, Y. In Vitro Selection of a Sodium-Specific DNAzyme and Its Application in Intracellular Sensing. *Proc. Natl. Acad. Sci. U. S. A.* **2015**, *112*, 5903−5908.
(48) Wu, Z.; Fan, H.; Satyavolu, N. S. R.; Wang, W.; Lake, R.; Jiang, J. H.; Lu, Y. Imaging Endogenous Metal Ions in Living Cells Using a DNAzyme-Catalytic Hairpin Assembly Probe. *Angew. Chem., Int. Ed.* **2017**, *56*, 8721−8725.
(49) McGhee, C. E.; Yang, Z.; Guo, W.; Wu, Y.; Lyu, M.; DeLong, C. J.; Hong, S.; Ma, Y.; McInnis, M. G.; O'Shea, K. S.; Lu, Y. DNAzyme-Based Lithium-Selective Imaging Reveals Higher Lithium Accumulation in Bipolar Disorder Patient-Derived Neurons. *ACS Cent. Sci.* **2021**, *7*, 1809−1820.
(50) Zhou, W.; Vazin, M.; Yu, T.; Ding, J.; Liu, J. In Vitro Selection of Chromium-Dependent DNAzymes for Sensing Chromium(III) and Chromium(VI). *Chemistry* **2016**, *22*, 9835−9840.
(51) Huang, P. J.; Vazin, M.; Liu, J. In Vitro Sselection of a New Lanthanide-Dependent DNAzyme for Ratiometric Sensing Lanthanides. *Anal. Chem.* **2014**, *86*, 9993−9999.
(52) Liu, M.; Chang, D.; Li, Y. Discovery and Biosensing Applications of Diverse RNA-Cleaving DNAzymes. *Acc. Chem. Res.* **2017**, *50*, 2273−2283.
(53) Yu, H.; Alkhamis, O.; Canoura, J.; Liu, Y.; Xiao, Y. Advances and Challenges in Small-Molecule DNA Aptamer Isolation, Characterization, and Sensor Development. *Angew. Chem., Int. Ed.* **2021**, *60*, 16800−16823.
(54) Canoura, J.; Yu, H.; Alkhamis, O.; Roncancio, D.; Farhana, R.; Xiao, Y. Accelerating Post-SELEX Aptamer Engineering Using Exonuclease Digestion. *J. Am. Chem. Soc.* **2021**, *143*, 805−816.
(55) Lake, R. J.; Yang, Z.; Zhang, J.; Lu, Y. DNAzymes as Activity-Based Sensors for Metal Ions: Recent Applications, Demonstrated Advantages, Current Challenges, and Future Directions. *Acc. Chem. Res.* **2019**, *52*, 3275−3286.
(56) Hollenstein, M.; Hipolito, C.; Lam, C.; Dietrich, D.; Perrin, D. M. A Highly Selective DNAzyme Sensor for Mercuric Ions. *Angew. Chem., Int. Ed.* **2008**, *47*, 4346−4350.
(57) Bruesehoff, P. J.; Li, J.; Augustine, A. J.; Lu, Y. Improving Metal Ion Specificity During in Vitro Selection of Catalytic DNA. *Comb. Chem. High Throughput Screening* **2002**, *5*, 327−335.
(58) Liu, J.; Lu, Y. Improving Fluorescent DNAzyme Biosensors by Combining Inter- and Intramolecular Quenchers. *Anal. Chem.* **2003**, *75*, 6666−6672.
(59) Zhou, W.; Saran, R.; Liu, J. Metal Sensing by DNA. *Chem. Rev.* **2017**, *117*, 8272−8325.
(60) Kumar, K. K.; Lowe, E. W., Jr.; Aboud, A. A.; Neely, M. D.; Redha, R.; Bauer, J. A.; Odak, M.; Weaver, C. D.; Meiler, J.; Aschner, M.; Bowman, A. B. Cellular Manganese Content Is Developmentally Regulated in Human Dopaminergic Neurons. *Sci. Rep.* **2014**, *4*, 6801.
(61) Schroeder, H. A.; Tipton, I. H. The Human Body Burden of Lead. *Arch. Environ. Health* **1968**, *17*, 965−978.
(62) Wang, Z.; Yang, J.; Qin, G.; Zhao, C.; Ren, J.; Qu, X. An Intelligent Nanomachine Guided by DNAzyme Logic System for Precise Chemodynamic Therapy. *Angew. Chem., Int. Ed.* **2022**, *61*, No. e202204291.
(63) Fan, H.; Zhao, Z.; Yan, G.; Zhang, X.; Yang, C.; Meng, H.; Chen, Z.; Liu, H.; Tan, W. A Smart DNAzyme-MnO_2 Nanosystem for Efficient Gene Silencing. *Angew. Chem., Int. Ed.* **2015**, *54*, 4801−4805.
(64) Wang, Z.; Niu, J.; Zhao, C.; Wang, X.; Ren, J.; Qu, X. A Bimetallic Metal-Organic Framework Encapsulated with DNAzyme for Intracellular Drug Synthesis and Self-Sufficient Gene Therapy. *Angew. Chem., Int. Ed.* **2021**, *60*, 12431−12437.
(65) Gavin, C. E.; Gunter, K. K.; Gunter, T. E. Mn^{2+} Sequestration by Mitochondria and Inhibition of Oxidative Phosphorylation. *Toxicol. Appl. Pharmacol.* **1992**, *115*, 1−5.
(66) Ding, B.; Zheng, P.; Jiang, F.; Zhao, Y.; Wang, M.; Chang, M.; Ma, P.; Lin, J. MnOx Nanospikes as Nanoadjuvants and Immunogenic Cell Death Drugs with Enhanced Antitumor Immunity and Antimetastatic Effect. *Angew. Chem., Int. Ed.* **2020**, *59*, 16381−16384.
(67) Lin, L. S.; Song, J.; Song, L.; Ke, K.; Liu, Y.; Zhou, Z.; Shen, Z.; Li, J.; Yang, Z.; Tang, W.; Niu, G.; Yang, H. H.; Chen, X. Simultaneous Fenton-like Ion Delivery and Glutathione Depletion by MnO_2-Based Nanoagent to Enhance Chemodynamic Therapy. *Angew. Chem., Int. Ed.* **2018**, *57*, 4902−4906.
(68) Yang, G.; Xu, L.; Chao, Y.; Xu, J.; Sun, X.; Wu, Y.; Peng, R.; Liu, Z. Hollow MnO_2 as a Tumor-Microenvironment-Responsive Biodegradable Nano-platform for Combination Therapy Favoring Antitumor Immune Responses. *Nat. Commun.* **2017**, *8*, 902.

https://doi.org/10.1021/jacsau.3c00062
JACS Au 2023, 3, 1615−1622